Experimental and ANN Analysis of Shearing Rate Effects on Coarse Sand Crushing

Samer R. Rabab'ah [1*] , Omar H. Al Hattamleh [2] , Ahmad N. Tarawneh [2] ,
Hussien H. Aldeeky [2]

[1] *Department of Civil Engineering, Jordan University of Science and Technology, P.O. Box 3030, Irbid, 22110, Jordan.*

[2] *Department of Civil Engineering, College of Engineering, The Hashemite University, P.O. Box 150459, Zarqa 13115, Jordan.*

Abstract

The present study analyzes laboratory experiments on how shearing rate affects the shear strength and crushability of natural coarse sand, employing artificial neural network (ANN) analysis. This study tested three different coarse sands obtained from the crushing of natural rocks: Black Virgin Tuff, weathered Zeolitic Tuff, and calcareous limestone. The behavior of crushed sand specimens with consistent grading, which passed through sieve #4 and were retained on sieve #8, was analyzed using a direct shear box. The specimens were subjected to varied normal loads and shearing speeds to examine their behavior at different relative densities. The test results were analyzed using ANN to investigate the significance of shearing rates on shearing strength parameters, specifically internal mobilized peak friction, the constant volume (residual) internal friction angle, and the consequence of shearing rate on the particle's breakage index. The selected normal (Gaussian) rate significantly affected both the shear strength parameters and breakage. The loading rate increased both shear strength parameters and particle breakage. Therefore, it's highly recommended to maintain secure sets of shear strength values and comprehensive test data for assessing parameters at typical strain rates, prioritizing using slower rates whenever possible.

Keywords: Coarse Sand; Direct Shear Box; Grain Breakage; Density Index; Shearing Rate; ANN.

1. Introduction

The breakage phenomenon in granular materials has garnered significant attention from researchers within the geotechnical community. This interest stems from the widespread use of granular materials in various engineering construction projects, such as rockfill dams, railroad embankments, landslides, and driven piles. These structures encounter diverse loading scenarios, ranging from static to dynamic forces, which can lead to complex behaviors and failure mechanisms in the granular materials [1–6]. Lobo-Guerrero and Vallejo (2005, 2006) [7, 8] examined the effect of particle crushing on the capacity of driven piles. Their results indicated that the particles crushing negatively affect the capacity of piles. Okada et al. (2004) [1] reported that grain crushing was at the onset of trigging a landslide. An investigation of the excess pore water pressure generation of weathered granitic sand, taken from the source area of a typical landslide caused as a result of liquefaction, indicated that grain crushing within the failure zone is the key phenomenon of the rapid long-runout motion of landslides. Moreover, Fragaszy & Voss (1986) [9] reported that particle breakage will cause settlements and a reduction in hydraulic conductivity.

The crushing process of granular materials has the potential to alter shear strength parameters over the lifespan of construction projects, posing a threat to the integrity and safety of the project. Therefore, engineers and project managers must anticipate and mitigate the effects of crushing on shear strength parameters to ensure the long-term safety and durability of construction projects. Incorporating appropriate design considerations, monitoring techniques, and maintenance protocols can help to address the evolving properties of granular materials and mitigate potential hazards throughout the project's lifespan.

Researchers aim to investigate the factors that affect particle crushing to develop accurate predictive models and engineering strategies for mitigating risks associated with granular materials in construction and geotechnical applications. These factors include various variables such as sand grain characteristics, soil matrix properties, fabric and structure of the soil domain, loading scenarios, and type of granular materials, among many other factors [5]. Karatza et al. (2019), Xiao et al. (2019), and Varadarajan et al. (2006) studied sand grain characteristics such as angularity, morphology, and strength [10–12]. Soil matrix properties such as gradation, void distribution, and moisture content were examined by [13–16]. The fabric and structure of the soil domain, such as anisotropy [17, 18], external forces such as induced stresses [19–21], duration [20], and loading rates [22, 23], were appraised immensely. Granular materials include sands, ballast, rock fill, coral**,** coal, and food powder such as sugar and snow [5, 19, 24–33]. The intensity of particle breakage is appraised through the variation of the grading of granular materials using single grading, either indices or global grading indices obtained from the particle size distribution curve (PSD) [5]. Table 1 summarizes the method of various single-grading indices.

Table 1. Definition of single grading indices

Method Name	Criteria[*]	Remarks
Lee & Farhoomand (1967)	$B_{15} = D_{15}^i / D_{15}^f$	D_{15} = particle size corresponding to 15% finer on PSD
Marsal (1967)	$B_g = \Delta P_{max}$	ΔP_{max} = maximum difference of the PSD curves before and after the test
Nakata et al. 1999	$B_f = 1 - P_0$	P_0= percentage of particles in current PSD smaller than the minimum particle size in the original sand
Xiao & Liu (2017)	$B_{r50} = (D_{50}^i - D_{50}^c)/(D_{50}^i - D_{50}^u)$	D_{50} =mean particle diameters

[*] i = initial; c = current, f = final, u = ultimate.

The global grading indices are evaluated through the changes in different areas bounded by ultimate, current, and initial PSD curves. Hardin (1985) and Einav (2007) are the most used criteria [34, 35]. Recently, Xiao et al. (2021) proposed an improved particle breakage index criterion to overcome the shortages of other criteria, such as the representation of all particle breakage in the whole domain, unique value, independent of grain side axis, and used in all types of gradation patterns [36].

Recently, there has been a noticeable shift in engineering modeling and computation toward machine learning techniques. In the last decade, machine-learning methods have been used in different fields of civil engineering [32–42] and have shown a high ability to recognize the pattern and relations between variables and the dependent. In particular, ANN mimics the interconnected nervous system of the human brain to transfer the data and recognize the pattern, as will be described in a later section.

The study is motivated by the observation that shear strength parameters, influenced by applied shear strain rate, lack relevant crushing indices when assessed across a wide range of relative initial density in crushed natural sands using conventional testing methods like triaxial compression or direct shear tests. Al-Hattamleh et al. (2023) [18] highlighted a significant gap in research concerning the examination of quasi-rates of applied shear strain on sand specimens. These quasi-rates of strain play a critical role in the development of crushing within granular materials. Yet, they are seldom explored in existing literature. Understanding the influence of these quasi-rates on the crushing behavior of granular materials is essential for accurately predicting their shear strength parameters.

This research aims to investigate the influence of normal shearing rates on breakage in various types of sands using a combination of experimental results and ANN analysis. This study will provide experimental data and analysis for these sand types to address a gap in the existing literature, particularly regarding black volcanic tuff and Zeolitic volcanic tuff and the associated shearing device methodologies. Additionally, it will outline the procedure for direct shear testing, offering valuable insights into the behavior of these sands under different shearing rates.

2. Experimental Works

2.1. Materials

Three types of sand were selected for this study: a Virgin Black Volcanic Tuff (BT), a weathered Zeolitic Volcanic Tuff (ZT), and Limestone (LT). The Al-Hala region in Al-Tafila in southern Jordan provided the BT and ZT sands. According to ASTM E1621-13 standard X-ray fluorescence spectroscopy examination, BT and ZT are both mostly constituted of SiO_2, ranging from 40% to 50%, with notable amounts of Fe_2O_3 and Al_2O_3 oxides, ranging from 12.75%

to 13.00% and from 10.67% to 12.64%, respectively. On the other hand, the Limestone (LS) was obtained from Irbid in northern Jordan. LS comprises nearly equal percentages of calcareous materials $CaCO_3$ and CaO (40-46%). The Specific gravity (Gs), Minimum Dry Density (ρ_{min}), and Maximum Dry Density (ρ_{max}) of all types of sands were conducted according to the American Society for Testing and Materials standards (ASTM) [38, 39], respectively. The Gs for BT, ZT, and LS are 2.67, 2.64, and 2.53, respectively. While the (ρ_{min} (kg/m^3), ρ_{max} (kg/m^3)) for BT, ZT, and LS are (1100, 1355), (900, 1030), and (1068, 1328), respectively. The grain sizes of the three varieties of sand were measured according to ASTM D6913 [40]. The grane size ranges utilized for the shear testing were specifically chosen to pass sieve #4 at 4.75mm and be retained at 2.36mm (sieve #8). Because the specimens are of the same grain size, the coefficient of uniformity and curvature are close to unity for all types of sand. As a result, the Unified Soil Classification System (USCS) classifies these sands as poorly graded sand, SP [41].

2.2. Test Setup

A direct, simple shear box (DSB) device was used to conduct the shearing of prepared specimens. The apparatus can apply vertical and horizontal forces up to 5 kN. Two linear variable differential transformers (LVDTs) measured the horizontal and vertical displacements. The device was designed to accommodate a cubical soil specimen of 6.00 cm side. The maximum grain size utilized in the test was selected to ensure that no boundary would alter the outcomes in compliance with ASTM D3080 [42] general requirements.

Dry samples of the four relative densities of the loose, medium, and very dense sand were subjected to DSB tests following ASTM D6528 [43] at three different loading rates (0.50, 1.00, and 2.00 mm/minute) under four different vertical stress conditions (136, 245, 463, and 899 kPa). Sieves analyses were performed for each test, and the results of all tests are summarized in Table 2. Data from DSB tests were analyzed to establish the shear strength parameters for each test, specifically constant volume (residual) mobilized friction angle (ϕ_r) and peak mobilized friction angle (ϕ_p). After performing the DSB test on each specimen, sieve analysis was used to determine the amount and percentage of particle breakage index (Br).
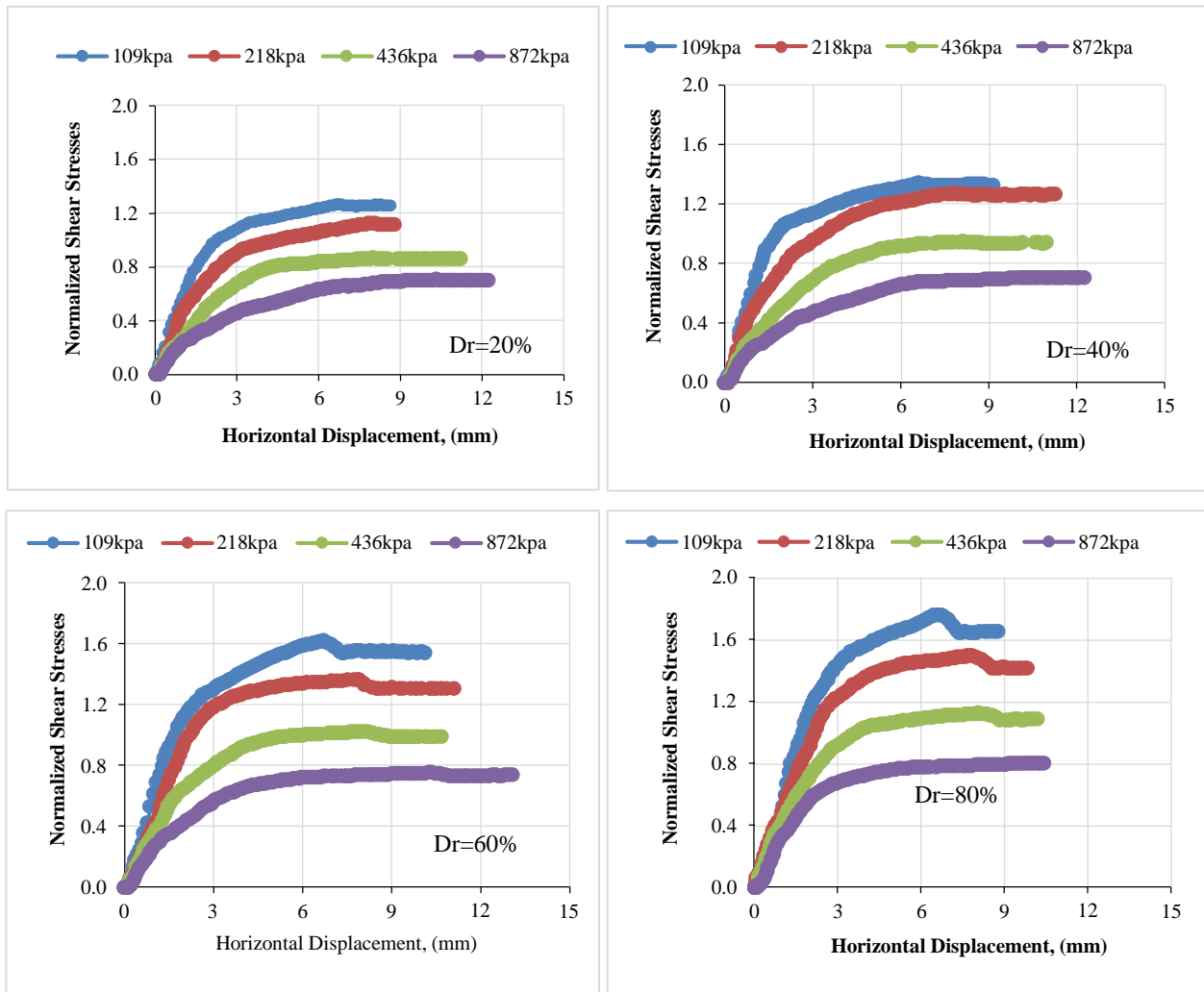
3. Results and Discussion

3.1. Experimental Results

The specimens were prepared for the DSB tests as described in Table 2. For BT sand at a shearing rate of mm/minutes, Figure 1 shows the relationship between normalized shear stresses and horizontal displacement of various relative densities. This figure shows that, as predicted, the shear stress arose as the shear displacement increased, reaching a peak value before decreasing to an asymptote value as the shear displacement increased. Sand particles moved rather easily under low normal stress conditions, and the relative displacement immediately stabilized. However, a bigger shear displacement was necessary to achieve a stable condition when the normal stress was high as it increased the contact between sand particles and made displacement more difficult.

Table 2. Summary of the conducted tests: Relative densities, applied vertical stresses, and applied shearing rates were used in tests for the sand in a direct shear test

Relative Density (%)	Density kg/m³			Vertical Stress, σ_v: kPa	Shearing Rate (mm/minute)	Remarks
	BT	ZT	LS			
20%	1143	996.8	1110	136	0.50, 1.00, & 2.00	
				245	0.50, 1.00, & 2.00	
				463	0.50, 1.00, & 2.00	
				899	0.50, 1.00, & 2.00	
40%	1190	1023.8	1023.8	136	0.50, 1.00, & 2.00	Sieve analyses were conducted after each test for all rates and applied vertical stresses.
				245	0.50, 1.00, & 2.00	
				463	0.50, 1.00, & 2.00	
				899	0.50, 1.00, & 2.00	
60%	1240	1051.9	105139	136	0.50, 1.00, & 2.00	
				245	0.50, 1.00, & 2.00	
				463	0.50, 1.00, & 2.00	
				899	0.50, 1.00, & 2.00	
80%	1129	1080	1270	136	0.50, 1.00, & 2.00	
				245	0.50, 1.00, & 2.00	
				463	0.50, 1.00, & 2.00	
				899	0.50, 1.00, & 2.00	

Figure 1. Normalized shear stresses vs. horizontal displacement of different relative densities for BT sand at a shearing rate of 0.50 mm/minutes

Moreover, as the relative density, Dr, increases and normal stresses decrease, a distinct peak is observed, and then, with further displacement, a softening occurs. These results are consistent with what Duncan et al. (2014) [44] assumed: the most crucial factors affecting soil strength are the effective stress applied to the soil and soil density. Thus, higher effective stress results in higher strength, and the higher the density, the higher the strength

The mobilized friction angles of the tested sands were calculated to assess the impact of using various shearing rates. The mobilized shear strength parameters ϕ_p and ϕ_r are defined as:

$$\phi_p = \tan^{-1} \frac{\tau_{peak}}{\sigma} \tag{1}$$

$$\phi_r = \tan^{-1} \frac{\tau_{residual}}{\sigma} \tag{2}$$

where τ_{peak}, $\tau_{residual}$, and applying normal stresses are the peak shearing stresses.

Based on global grading indices, the particle breakage index, Br, is reported here [5]. The Einav (2007) breakage index is determined using the grain size distribution curves before and after shearing. When sheared, the gradation curves change from a wide sieve opening to a smaller one. The ZT sand specimen's grain size distribution after direct shear testing with various normal stresses and relative density of Dr=80% at a loading rate of 1mm/min is shown in Figure 2.

3.2. Artificial Neural Network Model

In this study, an ANN was selected to assess the impact of shearing load, loading rate, and the relative density of sand on the peak internal friction angles, residual internal friction angles, and breakage index. ANN has been selected for its ability to generalize and avoid overfitting [45].

ANN is a multi-layer framework; the input layer of an ANN is the first layer, representing the parameters, while the output layer is the last, containing the output. One or more hidden layers may be present between the input and output

layers, controlling the process of identifying (learning) patterns in the data. Simple processing units (PUs) comprise each layer and are completely coupled to other PUs in the layer above them (Figure 3).
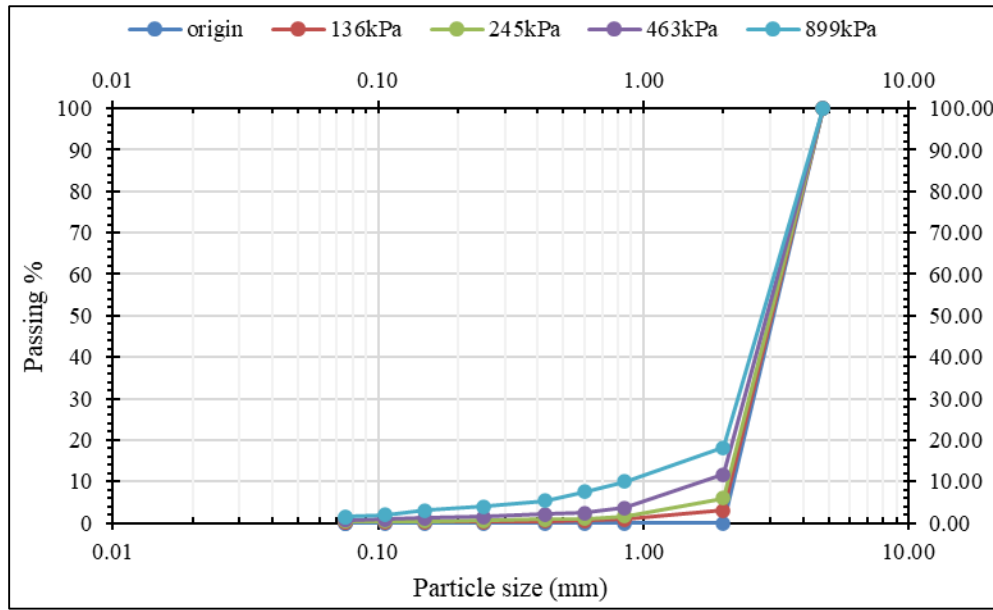

Figure 2. Sieve analysis for ZT at Dr=80%, Rate of Loading=1 mm/min, and different normal stress
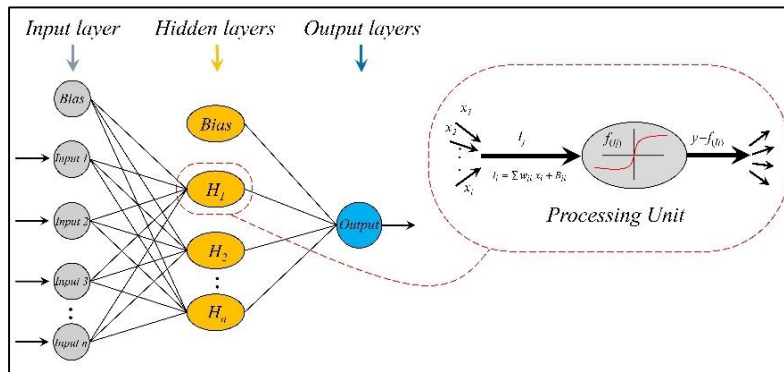

Figure 3. General structure and processing unit of ANNs

Whenever a signal or input x_i is received, the PU is multiplied by a calibrated weight w_{ji} that determines the signal's behavior and importance. Each PU adds the calibrated signals together and adds a calibrated bias value B_{ji} according to Equation 3. The output of the PU is produced by passing the combined input I_j using a nonlinear transfer function f(I_j), which will serve as the input for PUs in the following layer (Figure 3-b). This study makes use of a hyperbolic tangent sigmoid transfer function.

$$I_j = \sum w_{ji} \, x_i + B_{ji} \qquad (3)$$

The training algorithm modifies the weights and bias values of Levenberg-Marquardt optimization during the training process. In order to create a network that generalizes well, it first identifies the optimal combination of squared errors and weights. It is known as Bayesian regularization. The performance function, referred to as the Mean Square error (MSE), is used to express the error (Equation 4). Training continues until MSE converges and no further advancement in the solution is achieved.

$$MSE = \frac{1}{N} \sum_{k=1}^{N} (Actual - Predicted)^2 \qquad (4)$$

It should be noted that the first step required by Equation 5 is for the input variables to be normalized. The input value is shifted by the offset value of_{in} and multiplied by the gain value a_{in}. To de-normalize the signal at the output layer, remove the offset of_{on} and divide the output by the gain a_{on}.

$$x_i = X_i \, a_{in} + of_{in} \qquad (5)$$

Experimentation is used to determine the number of PUs needed in the hidden layer to mimic and approximate the complex behavior (trial). In ANN modeling, the number of hidden layers should often be limited to prevent overfitting. However, overfitting was not a concern due to using Bayesian regularization in the particular instance.

3.2.1. Proposed Models

Three ANN models were developed using the ANN toolbox of MATLAB R2018b. To select the optimal PUs in the hidden layer, PUs from 1 to 10 were tested while examining the MSE, and the optimal required number of layers was found to be 2. The experimental data has been divided into a training dataset (80%) and a validation dataset (20%). In this study, the input layer includes normalized period shearing load σn, loading rate, and soil Density (Dr.), while the output layer includes peak internal friction angles ϕ_p, residual internal friction angles ϕ_r, and the breakage index Br. The three ANN models and the corresponding R^2 are shown in Figure 4.
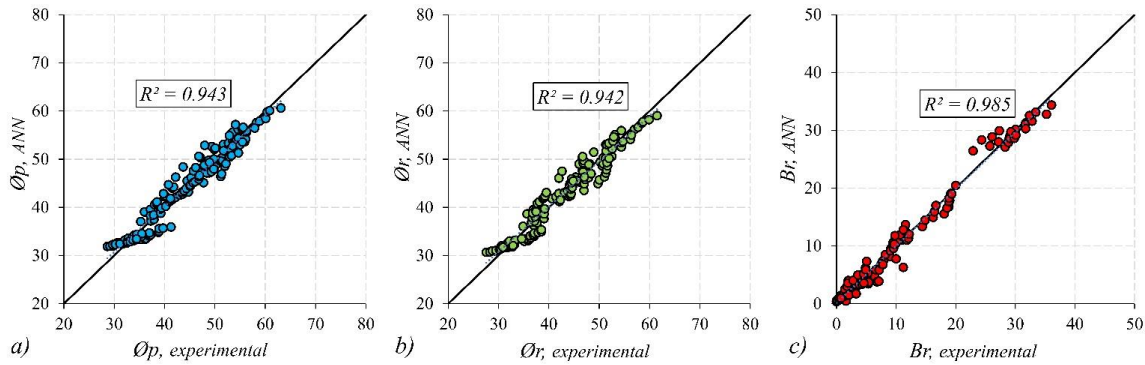
Figure 4. Developed ANN model to predict peak internal friction angles ϕp, residual internal friction angles ϕr, and the breakage index Br

In order to investigate the effect of each of the input layer variables, parametric curves were generated using the developed ANN models, as shown in Figure 5.
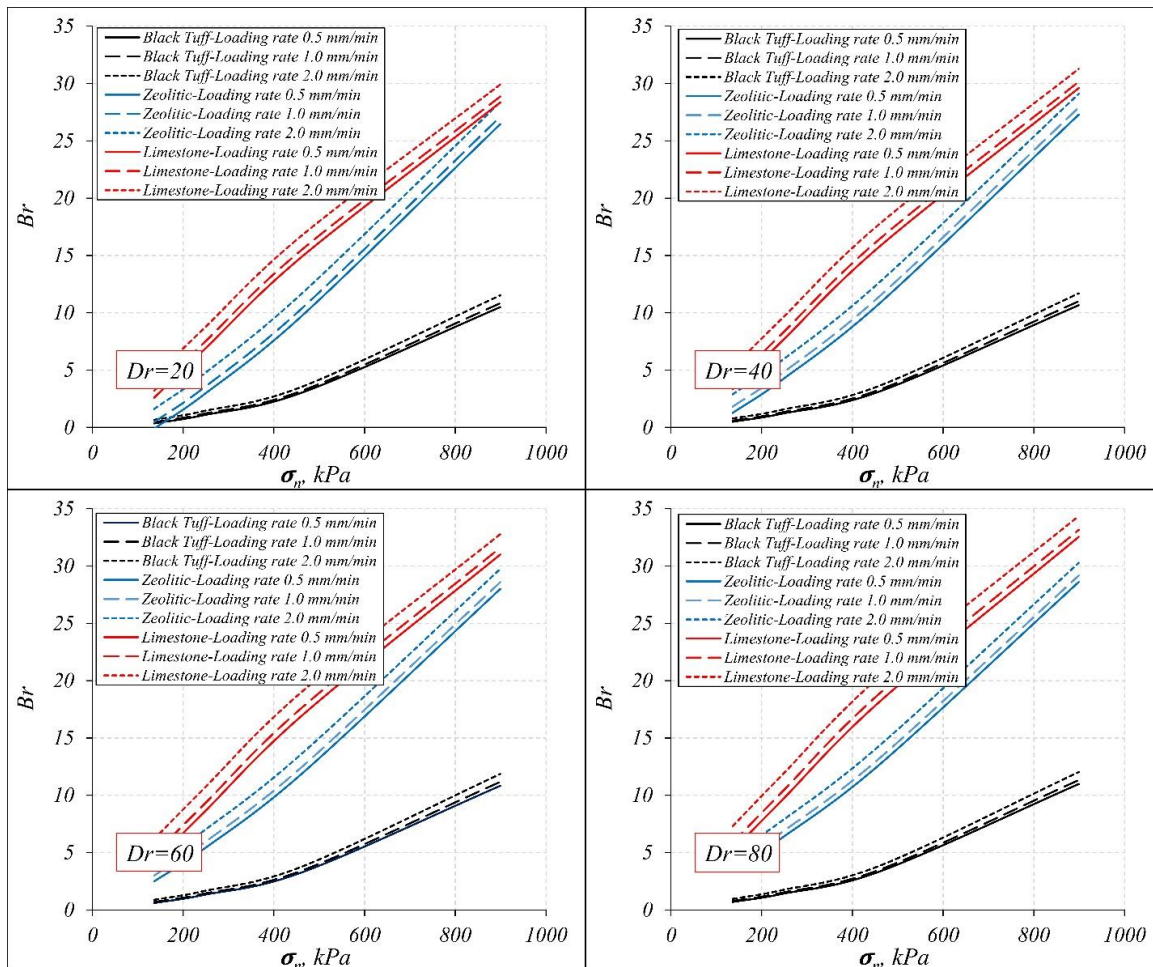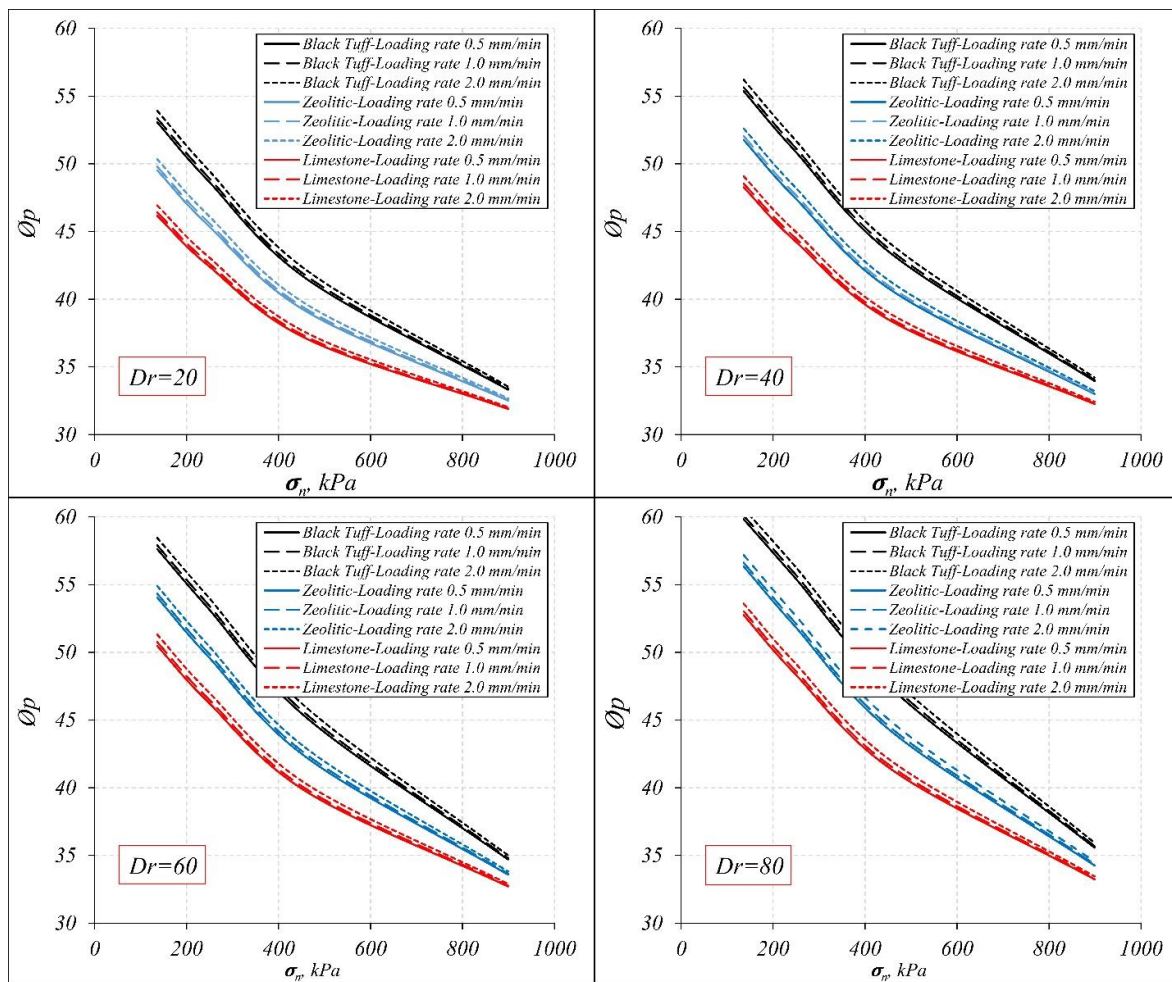

Figure 5. Particle Breakage Indices versus applied normal pressure for three types of sand at three different shearing rates for different relative densities

3.2.2. ANN Results and Discussion

Figure 5 shows the prediction of ANN models to the particle breakage indices, Br, as a function of normal applied stresses at a different shearing rate for sand specimens prepared at different relative densities. As anticipated, the amount of Br increased with the applied vertical stress and with higher relative density for all types of sands. This finding is rectified by Xiao et al. (2020) in a one-dimensional compression test for carbonate sand and by Asadzadeh and Soroush (2009) [46] for rockfill material composed of a limestone tested in direct shear such as LS here. Moreover, the particle breakage index shows a linear dependence on the applied normal stresses. regardless of the initial relative density (Figure 5) which was confirmed earlier by Asadzadeh & Soroush (2009) [46]. Conversely, for stronger materials like BT here, the particle breakage is more toward a power-like trend, as shown by Wang et al. (2021) [47].

Furthermore, the Br increases drastically with an increased rate of shearing at a given relative density despite the applied normal stress or type of sand. The reason was that the sand grains did not take enough time to rearrange or to orientate themselves, so the crushing of particles increased. Additionally, with D_r increasing, the amount of Br increased in all soil types tested. This finding was confirmed by many researchers [26, 48, 49], who showed that particle breakage is inversely proportional to the increased initial void ratio. The amount of crushing reported is higher for LS than BT and ZT sands due to weak bonds of $CaCO_3$ compared with SiO_2. This finding confirms what has been reported earlier in the literature, that crushing is directly related to particle strength [34, 50–52]. A rectification by Al-Hattamleh et al. (2023) [18], using scanning electron microscopy (SEM) supplied with energy-dispersive X-ray spectroscopy (SEM/EDX) of samples taken from the shearing zone of tested specimens, shows that the granules of original sizes which confined between 2.36 mm and 4.75 mm experience disintegration and cleavage, abrasion and grinding and surfaces' scratching.

Figure 6. Peak internal friction angles versus applied normal pressure for three types of sand at three different shearing rates for different relative densities

The prediction of ANN models for peak and residual internal friction angles is shown in Figures 6 and 7. Both figures show internal friction angles versus applied normal pressure for three types of sand at three different shearing rates for different relative densities. Both figures show that applied vertical stresses considerably lower peak and residual angles, independent of the sand samples' relative densities or the employed shear rate. The impact of exerting pressure and shearing rates, particularly at larger relative densities, are more or less reduced in residual friction angle. This result could explain the critical states line's downward migration in the compression plane [48, 49, 53, 54]. Moreover, the

effect of the shearing rate in both $\phi\tau\eta\varepsilon$ $_p$ angle (Figure 6) and ϕ_r angle (Figure 7) is pronounced. According to these findings, despite the relative density values being employed, increasing the shearing rate increased both ϕ_p and ϕ_r angles. On the other hand, a further increase in the shearing rate appeared to smooth out the growing degree of friction angles. Hence, as pointed out by Wei et al. (2021) [55], the residual shear strength decreased with increasing roundness and aspect ratio due to the effect of particle breakage. Congruently, the residual friction angles, ϕ_r, decreased with increasing applied normal stresses, as shown in Figure 7.
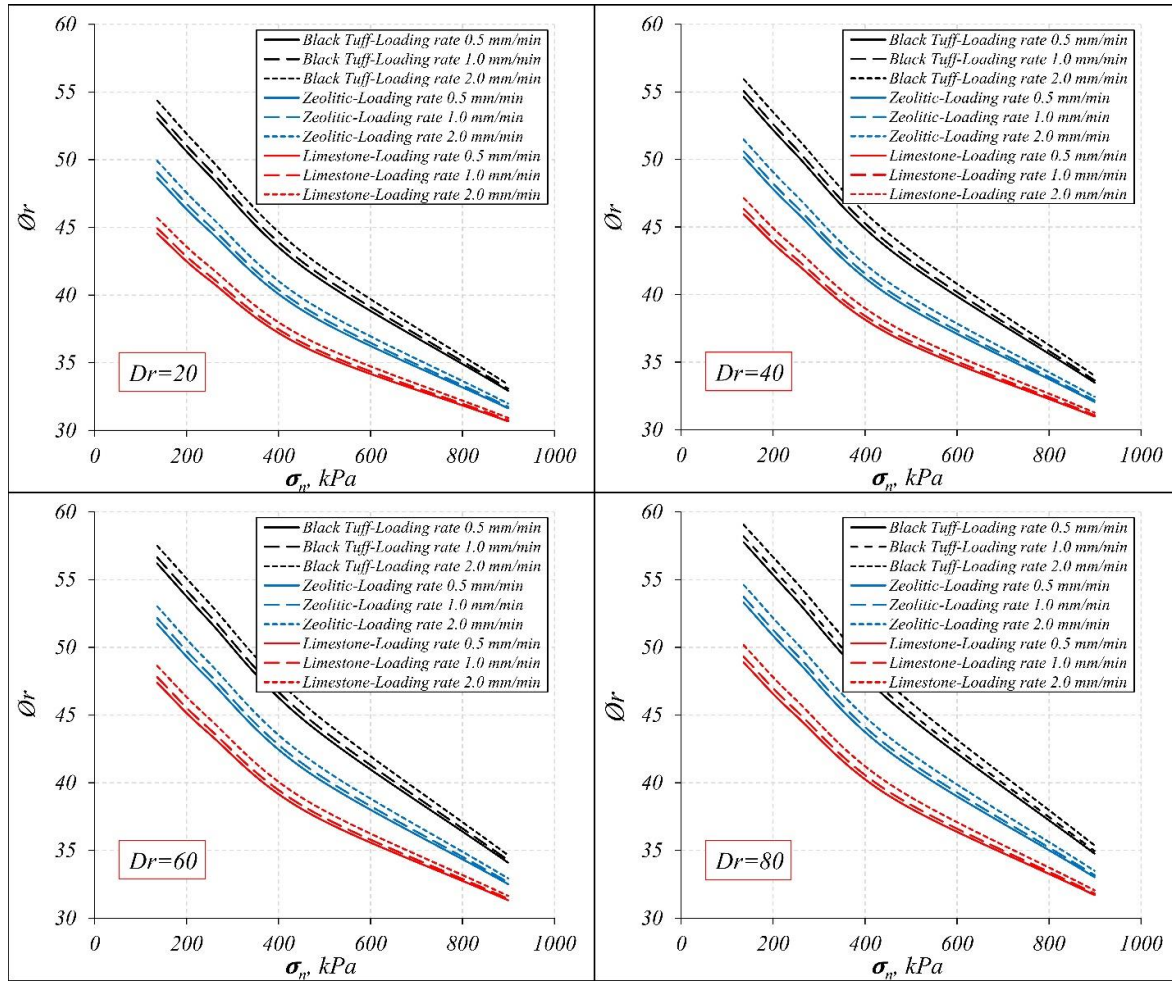

Figure 7. Residual internal friction angles versus applied normal pressure for three types of sand at three different shearing rates for different relative densities

4. Conclusions

The effect of the normal shearing rate was experimentally conducted using a direct shear device on prepared specimens of three different types of natural sand. After that, the results were analyzed using the ANN technique. The analysis includes the effect of the shearing rate on particle breakage indices and its effect on the outcome of internal peak and residual friction angles. Based on the ANN models and the parametric study, the following conclusion can be drawn:

- The interaction between relative density, normal stress, and particle crushing indices, Br, reveals insightful trends across all sand types investigated. With increasing normal stress, relative density, and shearing rate, the Br values show a noticeable increase. Additionally, as the rate of shearing increases, the peak friction angle exhibits a concurrent increase, indicative of a strengthening of interparticle contacts and resistance to shear deformation. On the other hand, results show that the residual friction angle decreases with reductions in relative density and applied normal loads, while it enhances with increasing rates of shearing. These results emphasize the sensitivity of residual friction to variations in these parameters, reflecting the evolving interparticle interactions within the sand samples.

- Moreover, the comparative analysis among sand types highlights distinctive characteristics. BT sand exhibits the highest internal peak friction angle value compared to ZT and LS sands, indicating its notable resistance to shear deformation. Conversely, the breakage index is highest for LS sand compared to BT and ZT sands, suggesting a greater tendency for particle fragmentation and degradation in LS sand. The contrasting behaviors observed highlight the varied mechanical responses of different types of sand under different loading conditions, emphasizing the importance of considering sand-specific properties in engineering and geotechnical applications.

5. Declarations

5.1. Author Contributions

Conceptualization, S.R., O.A., and H.A.; methodology, O.A. and A.T.; software, A.T.; writing—original draft preparation, S.R., O.A., and A.T; writing—review and editing, S.R. and O.A.; project administration, S.R., O.A., and H.A. All authors have read and agreed to the published version of the manuscript.

5.2. Data Availability Statement

The data presented in this study are available on request from the corresponding author.

5.3. Funding

The authors received no financial support for the research, authorship, and/or publication of this article.

5.4. Conflicts of Interest

The authors declare no conflict of interest.

6. References

[1] Okada, Y., Sassa, K., & Fukuoka, H. (2004). Excess pore pressure and grain crushing of sands by means of undrained and naturally drained ring-shear tests. Engineering Geology, 75(3–4), 325–343. doi:10.1016/j.enggeo.2004.07.001.

[2] Sevi, A., & Ge, L. (2012). Cyclic Behaviors of Railroad Ballast within the Parallel Gradation Scaling Framework. Journal of Materials in Civil Engineering, 24(7), 797–804. doi:10.1061/(asce)mt.1943-5533.0000460.

[3] Kermani, M., Konrad, J.-M., & Smith, M. (2018). In Situ Short-Term and Long-Term Rockfill Compressibility as a Function of Void Ratio and Strength of Parent Rock. Journal of Geotechnical and Geoenvironmental Engineering, 144(4), 04018009. doi:10.1061/(asce)gt.1943-5606.0001835.

[4] Altuhafi, F. N., Jardine, R. J., Georgiannou, V. N., & Moinet, W. W. (2018). Effects of particle breakage and stress reversal on the behaviour of sand around displacement piles. Geotechnique, 68(6), 546–555. doi:10.1680/jgeot.17.P.117.

[5] Xiao, Y., Desai, C. S., Daouadji, A., Stuedlein, A. W., Liu, H., & Abuel-Naga, H. (2020). Grain crushing in geoscience materials–Key issues on crushing response, measurement and modeling: Review and preface. Geoscience Frontiers, 11(2), 363–374. doi:10.1016/j.gsf.2019.11.006.

[6] Wang, Y., Cheng, Y., Yang, G., Xie, Y., Huang, H., & Liu, R. (2024). Study on the inhibitory effect of rubber on particle breakage and the impact on the volumetric deformation of calcareous sand under different loading modes. Construction and Building Materials, 414, 135014. doi:10.1016/j.conbuildmat.2024.135014.

[7] Lobo-Guerrero, S., & Vallejo, L. E. (2006). Modeling granular crushing in ring shear tests: Experimental and numerical analyses. Soils and Foundations, 46(2), 147–157. doi:10.3208/sandf.46.147.

[8] Lobo-Guerrero, S., & Vallejo, L. E. (2005). Crushing a weak granular material: Experimental numerical analyses. Geotechnique, 55(3), 245–249. doi:10.1680/geot.2005.55.3.245.

[9] Fragaszy, R. J., & Voss, M. E. (1986). Undrained compression behavior of sand. Journal of Geotechnical Engineering, 112(3), 334–347. doi:10.1061/(ASCE)0733-9410(1986)112:3(334).

[10] Karatza, Z., Andò, E., Papanicolopulos, S. A., Viggiani, G., & Ooi, J. Y. (2019). Effect of particle morphology and contacts on particle breakage in a granular assembly studied using X-ray tomography. Granular Matter, 21(3), 1-13. doi:10.1007/s10035-019-0898-2.

[11] Xiao, Y., Long, L., Matthew Evans, T., Zhou, H., Liu, H., & Stuedlein, A. W. (2019). Effect of Particle Shape on Stress-Dilatancy Responses of Medium-Dense Sands. Journal of Geotechnical and Geoenvironmental Engineering, 145(2), 04018105. doi:10.1061/(asce)gt.1943-5606.0001994.

[12] Varadarajan, A., Sharma, K. G., Abbas, S. M., & Dhawan, A. K. (2006). Constitutive Model for Rockfill Materials and Determination of Material Constants. International Journal of Geomechanics, 6(4), 226–237. doi:10.1061/(asce)1532-3641(2006)6:4(226).

[13] Hyodo, M., Wu, Y., Aramaki, N., & Nakata, Y. (2017). Undrained monotonic and cyclic shear response and particle crushing of silica sand at low and high pressures. Canadian Geotechnical Journal, 54(2), 207–218. doi:10.1139/cgj-2016-0212.

[14] Ovalle, C., & Hicher, P. Y. (2020). Modeling the effect of wetting on the mechanical behavior of crushable granular materials. Geoscience Frontiers, 11(2), 487–494. doi:10.1016/j.gsf.2019.06.009.

[15] Alonso, E. E., Romero, E. E., & Ortega, E. (2016). Yielding of rockfill in relative humidity-controlled triaxial experiments. Acta Geotechnica, 11(3), 455–477. doi:10.1007/s11440-016-0437-9.

[16] Xiao, Y., Meng, M., Wang, C., Wu, H., Fang, Q., & Liu, S. (2023). Breakage critical state of gravels with different gradings. Part I: Experimental results. Transportation Geotechnics, 42, 101087. doi:10.1016/j.trgeo.2023.101087.

[17] Al-Hattamleh, O. H., Al-Deeky, H. H., & Akhtar, M. N. (2013). The Consequence of Particle Crushing in Engineering Properties of Granular Materials. International Journal of Geosciences, 04(07), 1055–1060. doi:10.4236/ijg.2013.47099.

[18] Al-Hattamleh, O., Sharo, A., Abu Shanab, L., Aldeeky, H., & Al Dwairi, R. (2023). Effect of the quasi rate of loading in Particle Crushing and Engineering Properties of Black Tough Sand. Acta Montanistica Slovaca, 28(2), 301–313. doi:10.46544/AMS.v28i2.04.

[19] Al-Hattamleh, O., Alshalabi, F., Al Qablan, H., & Al-Rousan, T. (2010). Effect of grain crushing and bedding plane inclination on Aqaba sand behavior. Bulletin of Engineering Geology and the Environment, 69(1), 41–49. doi:10.1007/s10064-009-0238-6.

[20] Fu, Z., Chen, S., Zhong, Q., & Zhang, Y. (2019). Modeling interaction between loading-induced and creep strains of rockfill materials using a hardening elastoplastic constitutive model. Canadian Geotechnical Journal, 56(10), 1380–1394. doi:10.1139/cgj-2018-0435.

[21] Li, J., Huang, Y., Ouyang, S., Guo, Y., Gao, H., Wu, L., Shi, Y., & Zhu, L. (2022). Transparent characterization and quantitative analysis of broken gangue's 3D fabric under the bearing compression. International Journal of Mining Science and Technology, 32(2), 335–345. doi:10.1016/j.ijmst.2021.11.013.

[22] Huang, J. Y., Hu, S. S., Xu, S. L., & Luo, S. N. (2017). Fractal crushing of granular materials under confined compression at different strain rates. International Journal of Impact Engineering, 106, 259–265. doi:10.1016/j.ijimpeng.2017.04.021.

[23] Parab, N. D., Guo, Z., Hudspeth, M. C., Claus, B. J., Fezzaa, K., Sun, T., & Chen, W. W. (2017). Fracture mechanisms of glass particles under dynamic compression. International Journal of Impact Engineering, 106, 146–154. doi:10.1016/j.ijimpeng.2017.03.021.

[24] Yamamuro, J. A., Bopp, P. A., & Lade, P. V. (1996). One-Dimensional Compression of Sands at High Pressures. Journal of Geotechnical Engineering, 122(2), 147–154. doi:10.1061/(asce)0733-9410(1996)122:2(147).

[25] Miura, S., Yagi, K., & Asonuma, T. (2003). Deformation-strength evaluation of crushable volcanic soils by laboratory and in-situ testing. Soils and Foundations, 43(4), 47–57. doi:10.3208/sandf.43.4_47.

[26] Barraclough, T. W., Blackford, J. R., Liebenstein, S., Sandfeld, S., Stratford, T. J., Weinländer, G., & Zaiser, M. (2017). Propagating compaction bands in confined compression of snow. Nature Physics, 13(3), 272–275. doi:10.1038/nphys3966.

[27] Strahler, A. W., Stuedlein, A. W., & Arduino, P. (2018). Three-Dimensional Stress-Strain Response and Stress-Dilatancy of Well-Graded Gravel. International Journal of Geomechanics, 18(4), 04018014. doi:10.1061/(asce)gm.1943-5622.0001118.

[28] Yu, F. (2017). Particle Breakage and the Drained Shear Behavior of Sands. International Journal of Geomechanics, 17(8), 04017041. doi:10.1061/(asce)gm.1943-5622.0000919.

[29] Xiao, Y., Liu, H., Chen, Q., Ma, Q., Xiang, Y., & Zheng, Y. (2017). Particle breakage and deformation of carbonate sands with wide range of densities during compression loading process. Acta Geotechnica, 12(5), 1177–1184. doi:10.1007/s11440-017-0580-y.

[30] Zhang, J., Li, M., Liu, Z., & Zhou, N. (2017). Fractal characteristics of crushed particles of coal gangue under compaction. Powder Technology, 305, 12–18. doi:10.1016/j.powtec.2016.09.049.

[31] Indraratna, B., Ngo, T., & Rujikiatkamjorn, C. (2020). Performance of Ballast Influenced by Deformation and Degradation: Laboratory Testing and Numerical Modeling. International Journal of Geomechanics, 20(1), 04019138. doi:10.1061/(asce)gm.1943-5622.0001515.

[32] Yang, L., Long, Z., Kuang, D., Liu, X., & Li, Z. (2023). Influences of size, shape and strain rate on mechanical properties of single coral particle. Journal of Building Engineering, 78, 107667. doi:10.1016/j.jobe.2023.107667.

[33] Chen, J., Liu, Y., Hu, Q., & Gao, R. (2023). Effects of Particle Size and Grading on the Breakage of Railway Ballast: Laboratory Testing and Numerical Modeling. Sustainability, 15(23), 16363. doi:10.3390/su152316363.

[34] Hardin, B. O. (1985). Crushing of soil particles. Journal of Geotechnical Engineering, 111(10), 1177–1192. doi:10.1061/(ASCE)0733-9410(1985)111:10(1177).

[35] Einav, I. (2007). Breakage mechanics-Part I: Theory. Journal of the Mechanics and Physics of Solids, 55(6), 1274–1297. doi:10.1016/j.jmps.2006.11.003.

[36] Xiao, Y., Wang, C., Wu, H., & Desai, C. S. (2021). New Simple Breakage Index for Crushable Granular Soils. International Journal of Geomechanics, 21(8). doi:10.1061/(asce)gm.1943-5622.0002091.

[37] Chen, Q., Li, Z., Dai, Z., Wang, X., Zhang, C., & Zhang, X. (2023). Mechanical behavior and particle crushing of irregular granular material under high pressure using discrete element method. Scientific Reports, 13(1), 7843. doi:10.1038/s41598-023-35022-w.

[38] ASTM D854-23. (2023). Test Methods for Specific Gravity of Soil Solids by Water Displacement Method. ASTM International, Pennsylvania, United States. doi:10.1520/D0854-23.

[39] ASTM D7382-20. (2020). Standard Test Methods for Determination of Maximum Dry Unit Weight and Water Content Range for Effective Compaction of Granular Soils Using a Vibrating Hammer. ASTM International, Pennsylvania, United States. doi:10.1520/D7382-20.

[40] ASTM D6913-04(2009)E1. (2017). Standard Test Methods for Particle-Size Distribution (Gradation) of Soils Using Sieve Analysis. ASTM International, Pennsylvania, United States. doi:10.1520/D6913-04R09E01.

[41] ASTM D2487-17. (2020). Practice for Classification of Soils for Engineering Purposes (Unified Soil Classification System). ASTM International, Pennsylvania, United States. doi:10.1520/D2487-17.

[42] ASTM D3080-04. (2012). Test Method for Direct Shear Test of Soils Under Consolidated Drained Conditions. ASTM International, Pennsylvania, United States. doi:10.1520/D3080-04.

[43] ASTM D6528-17. (2017). Test Method for Consolidated Undrained Direct Simple Shear Testing of Cohesive Soils. ASTM International, Pennsylvania, United States. doi:10.1520/D6528-17.

[44] Duncan, J. M., Wright, S. G., & Brandon, T. L. (2014). Soil strength and slope stability. John Wiley & Sons, Hoboken, United States.

[45] Tarawneh, A., Almasabha, G., & Murad, Y. (2022). ColumnsNet: Neural Network Model for Constructing Interaction Diagrams and Slenderness Limit for FRP-RC Columns. Journal of Structural Engineering, 148(8), 04022089. doi:10.1061/(asce)st.1943-541x.0003389.

[46] Asadzadeh, M., & Soroush, A. (2009). Direct shear testing on a rockfill material. Arabian Journal for Science and Engineering, 34(2 B), 379–396.

[47] Wang, G., Wang, Z., Ye, Q., & Zha, J. (2021). Particle breakage evolution of coral sand using triaxial compression tests. Journal of Rock Mechanics and Geotechnical Engineering, 13(2), 321–334. doi:10.1016/j.jrmge.2020.06.010.

[48] Li, G., Liu, Y.-J., Dano, C., & Hicher, P.-Y. (2015). Grading-Dependent Behavior of Granular Materials: From Discrete to Continuous Modeling. Journal of Engineering Mechanics, 141(6), 04014172. doi:10.1061/(asce)em.1943-7889.0000866.

[49] Xiao, Y., & Liu, H. (2017). Elastoplastic Constitutive Model for Rockfill Materials Considering Particle Breakage. International Journal of Geomechanics, 17(1), 04016041. doi:10.1061/(asce)gm.1943-5622.0000681.

[50] McDowell, G. R., & Bolton, M. D. (1998). On the micromechanics of crushable aggregates. Geotechnique, 48(5), 667–679. doi:10.1680/geot.1998.48.5.667.

[51] Lade, P. V., Yamamuro, J. A., & Bopp, P. A. (1996). Significance of Particle Crushing in Granular Materials. Journal of Geotechnical Engineering, 122(4), 309–316. doi:10.1061/(asce)0733-9410(1996)122:4(309).

[52] Feda, J. (2002). Notes on the effect of grain crushing on the granular soil behaviour. Engineering Geology, 63(1–2), 93–98. doi:10.1016/S0013-7952(01)00072-2.

[53] Liu, M., Gao, Y., & Liu, H. (2014). An elastoplastic constitutive model for rockfills incorporating energy dissipation of nonlinear friction and particle breakage. International Journal for Numerical and Analytical Methods in Geomechanics, 38(9), 935–960. doi:10.1002/nag.2243.

[54] Ning, F., Liu, J., Kong, X., & Zou, D. (2020). Critical State and Grading Evolution of Rockfill Material under Different Triaxial Compression Tests. International Journal of Geomechanics, 20(2), 04019154. doi:10.1061/(asce)gm.1943-5622.0001550.

[55] Wei, H., Yin, M., Zhao, T., Yan, K., Shen, J., Meng, Q., Wang, X., & He, J. (2021). Effect of particle breakage on the shear strength of calcareous sands. Marine Geophysical Research, 42(3), 1-11. doi:10.1007/s11001-021-09440-2.